

PAPER • OPEN ACCESS

## Development of multi-depth probing 3D microelectrode array to record electrophysiological activity within neural cultures



To cite this article: Neeraj Yadav *et al* 2023 *J. Micromech. Microeng.* **33** 115002

View the [article online](#) for updates and enhancements.

You may also like

- [Wearable carbon nanotube based dry-electrodes for electrophysiological sensors](#)  
Byeong-Cheol Kang and Tae-Jun Ha
- [Measuring the electrophysiological effects of direct electrical stimulation after awake brain surgery](#)  
M A Vincent, F Bonnetblanc, E Mandonnet et al.
- [Simultaneous recording of the action potential and its whole-cell associated ion current on NG108-15 cells cultured over a MWCNT electrode](#)  
I Morales-Reyes, A Seseña-Rubfiaro, M C Acosta-García et al.

# Development of multi-depth probing 3D microelectrode array to record electrophysiological activity within neural cultures

Neeraj Yadav<sup>1,2,\*</sup> , Donatella Di Lisa<sup>3</sup>, Flavio Giacomozzi<sup>2</sup> , Alessandro Cian<sup>2</sup>, Damiano Giubertoni<sup>2</sup>, Sergio Martinoia<sup>3</sup> and Leandro Lorenzelli<sup>2</sup>

<sup>1</sup> Department of Industrial Engineering, University of Trento, Trento, Italy

<sup>2</sup> Center for Sensors & Devices (SD), FBK—Foundation Bruno Kessler, Trento, Italy

<sup>3</sup> Department of Informatics, Bioengineering, Robotics and Systems Engineering (DIBRIS), University of Genova, Genova, Italy

E-mail: [neeraj.yadav@unitn.it](mailto:neeraj.yadav@unitn.it)

Received 31 July 2023, revised 29 August 2023

Accepted for publication 13 September 2023

Published 22 September 2023



CrossMark

## Abstract

Microelectrode arrays (MEAs) play a crucial role in investigating the electrophysiological activities of neuronal populations. Although two-dimensional neuronal cell cultures have predominated in neurophysiology in monitoring *in-vitro* the electrophysiological activity, recent research shifted toward culture using three-dimensional (3D) neuronal network structures for developing more sophisticated and realistic neuronal models. Nevertheless, many challenges remain in the electrophysiological analysis of 3D neuron cultures, among them the development of robust platforms for investigating the electrophysiological signal at multiple depths of the 3D neurons' networks. While various 3D MEAs have been developed to probe specific depths within the layered nervous system, the fabrication of microelectrodes with different heights, capable of probing neural activity from the surface as well as from the different layers within the neural construct, remains challenging. This study presents a novel 3D MEA with microelectrodes of different heights, realized through a multi-stage mold-assisted electrodeposition process. Our pioneering platform allows meticulous control over the height of individual microelectrodes as well as the array topology, paving the way for the fabrication of 3D MEAs consisting of electrodes with multiple heights that could be tailored for specific applications and experiments. The device performance was characterized by measuring electrochemical impedance, and noise, and capturing spontaneous electrophysiological activity from neurospheroids derived from human induced pluripotent stem cells. These evaluations unequivocally validated the significant potential of our innovative multi-height 3D MEA as an avant-garde platform for *in vitro* 3D neuronal studies.

\* Author to whom any correspondence should be addressed.



Original content from this work may be used under the terms of the [Creative Commons Attribution 4.0 licence](https://creativecommons.org/licenses/by/4.0/). Any further distribution of this work must maintain attribution to the author(s) and the title of the work, journal citation and DOI.

Supplementary material for this article is available [online](#)

Keywords: multilevel, arrays, multi-electrodes, neuronal, electrophysiology, brain, *in vitro*

(Some figures may appear in colour only in the online journal)

## 1. Introduction

Understanding the structural and functional complexity of the human brain in health and disease represents one of the most critical challenges in neuroscience to study and develop treatments for neurodevelopmental disorders and neurodegenerative diseases [1–3]. Classical non-invasive *in vivo* approaches, such as imaging and electroencephalography, address this complexity in intact brains and allow studying physiologically active and pathologically dysfunctional circuits, but have limitations in spatial and temporal resolution, depth specificity and connectivity information [4–8]. Thus, alternative non-invasive models are required to dissect the cellular mechanisms underlying brain complexity in physiological and pathological conditions. In this respect, innovative and advanced *in vitro* models mimicking the brain's complex architecture are unique tools for investigating neuronal circuitry and function. More specifically, *in vitro* models allow detailed electrophysiological characterization of neuronal transmission and large-scale drug screening, which is not easily carried out *in vivo* [9, 10]. Several different types of *in vitro* neuronal models mimicking the complexity of neural circuits and reflecting the complex underpinnings of neurodevelopmental disorders are under intensive investigation, and researchers are shifting from two-dimensional (2D) network models to three-dimensional (3D) structures and organoids [11–15].

Numerous studies have been devoted to studying 3D-engineered neuronal networks coupled to 2D microelectrode arrays (MEAs) [16–19]. However, the existing 2D MEAs are inadequate to record the electrophysiological activity of 3D cellular networks from different locations in the 3D space, since the signal is recorded primarily from the layer directly coupled to the planar MEAs (figure 1(a)) [17]. The possibility to perform 3D mapping of neural networks can facilitate the study of spatio-temporal dynamics in electrophysiological signals and to identify correlations in neural activities. Thus, a new generation of 3D MEAs can allow the realization of experimental platforms based on a 3D neuron-device coupling, able to provide more realistic models in neurophysiology [20–22]. Despite the great demand, there is still a lack of sophisticated and robust technologies for 3D MEAs. The primary limitations deal with the realization of sufficiently reliable and economically sustainable solutions, offering compatibility with the existing experimental platforms in neurophysiology. To this end, numerous 3D MEAs have been developed using various fabrication technologies, leading to substantial improvements in electrode density and aspect ratio; however, the diversity of cell types and device applications necessitates an ideal 3D MEA device with configurable electrode geometry, density, aspect ratio, and array

topology [23–34]. A promising step in this direction could be a 3D MEA consisting of partially insulated microstructures with varying and precisely controlled heights of the electrodes [35, 36]. The state-of-the-art approaches are based on 3D micro-fabricated structures with embedded microelectrodes positioned at different heights, often conceived as top-down designs leading to stand-alone solutions independent from the specific neurophysiological experimental needs (figure 1(d)) [37, 38].

In the present study, we demonstrate an innovative technological platform for developing multi-height 3D MEA (MH-MEA) with four different electrode heights, capable of recording electrophysiological activities from different depths within the 3D neural culture. This process, founded on photolithography and a mold-assisted electrodeposition technique, facilitates the fabrication of microelectrodes with distinct heights. The structural properties of the device were characterized by optical profilometry and scanning electron microscopy (SEM). Electrochemical impedance spectroscopy was utilized to characterize the electrical properties of the microelectrodes. The device's feasibility was assessed by measuring individual electrode noise and recording spontaneous electrophysiological activity from a 3D human neurospheroid derived from the differentiation of human induced pluripotent stem cells (h-iPSCs). Furthermore, we compared the data from our multi-depth probing MH-MEA with the state-of-the-art 3D MEA with single-height electrodes (configuration similar to figure 1(c)) (referred to as 3D MC). Comparison tests were conducted under similar experimental conditions to ensure consistency.

## 2. Methods

### 2.1. Device fabrication

The fabrication process was carried out in a class 1000 clean-room using 150 mm polished borosilicate glass wafers from Plan Optik AG, Germany. A chrome/gold (Cr/Au) layer with a 10/200 nm thickness was deposited on the wafer using an ultralow vacuum electron beam evaporator (figure 2(a)). The wafer was then primed with hexamethyldisilazane at 150 °C to enhance photoresist adhesion. Followed by spin coating photoresist (OIR 305–20HC from Fujifilm) and soft-bake at 100 °C (figure 2(b)). The pattern was transferred from the mask to the photoresist using an i-line mask aligner (KARL SUSS MA6), followed by photoresist development and hardening (figure 2(c)). Subsequently, the metal layers were etched using wet chemical etching, thus completing the pattern transfer from the resist to the substrate. Finally, the photoresist was stripped using acetone, and the wafer

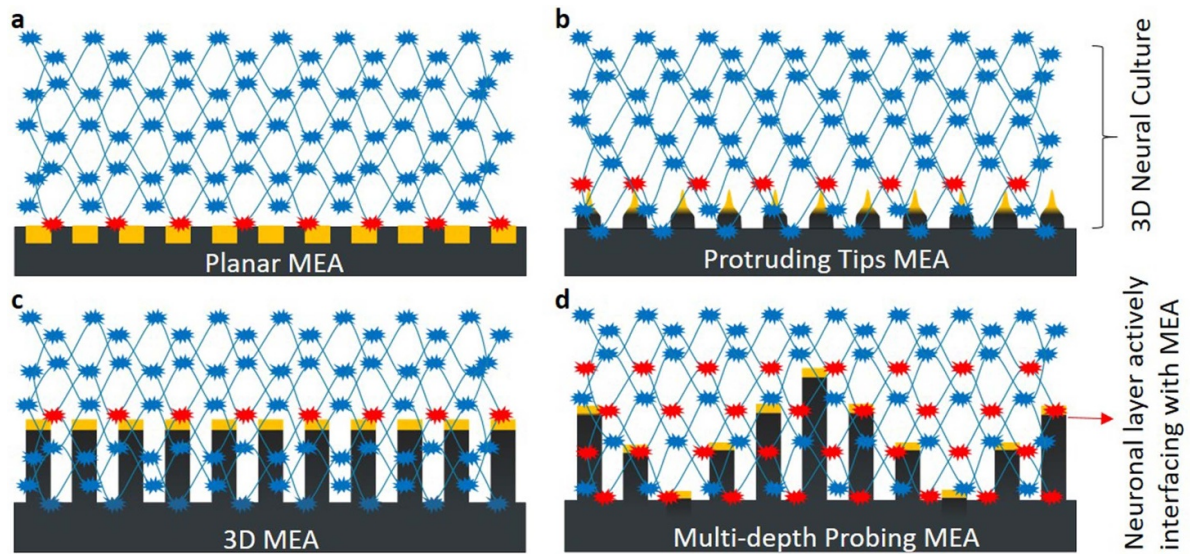


**Figure 1.** Schematic illustration of different types of MEAs interfacing with 3D neural cultures. (a): Planar MEAs limited to map electrical activity only from the surface layer of the 3D neural culture. (b): Protruding tip-based MEAs capable of interfacing neuronal layers adjacent to the surface. (c): 3D MEAs with single height electrodes capable of mapping activity from deep within the neuronal culture but limited to a single plane. (d): Multi-depth probing MEA consisting of electrodes with multiple heights enabling recoding of electrical activity from surface as well as multiple depths within the neural culture.

underwent sintering at 200 °C for 60 min (figure 2(d)). A 250 nm-thick passivation layer ( $\text{SiO}_2$ ) was deposited using plasma-enhanced chemical vapor deposition (figure 2(e)). The passivation layer was removed from the top of electrode and contact pads using reactive ion etching (TEGAL 903) (figures 2(f)–(i)). Upon realizing partially passivated planar MEAs, the wafer was coated with a 110  $\mu\text{m}$ -thick layer of chemically amplified negative photoresist (KMPR-1035, Kayaku Advanced Materials, Inc.) (Figure 2(j)). The photoresist was then exposed and developed, yielding a mold featuring 110  $\mu\text{m}$  deep cylindrical holes aligned over the planar electrodes (figure 2(k)).

The devices were then subjected to mold-assisted electrodeposition of gold micro-pillars (figure 2(l)). The gold micro-pillars were electrodeposited with a current density of 2  $\text{mA cm}^{-2}$  using an additive-free AUROLYTE CN200 (Atotech Deutschland GmbH & Co. KG) plating solution with temperature maintained at 55 °C. The selective electrodeposition process allowed for the deposition of gold micro-pillars with different heights, described in figure 3. Upon completion of the electrodeposition process, the photoresist mold was stripped using the mr-Rem 700 (micro resist technology) (figure 2(m)). Further, the sidewalls of the micro-pillars were passivated by depositing a 900 nm-thick Parylene-C layer using chemical vapor deposition (figure 2(n)), and selectively removed Parylene-C from the head of the electrodes (figure 2(o)). The sidewall passivation process is described in detail in appendix A (figure A2) of supplementary materials. Finally, the 3D MEA was packaged onto a customized printed circuit board compatible with the readout system.

## 2.2. Electrochemical measurements

The impedance of individual electrodes is determined using a two-electrode configuration impedance analyzer (HP4192—LF impedance analyzer). These measurements occurred within the 1–100 kHz range, employing a platinum counter electrode in an electrolytic solution (Cryson) at pH 7. Noise measurements were performed by recording the electrical activity of the electrodes in a PBS buffer solution and medium culture (neurobasal medium) at 10 kHz for 2 min using ME2100-System (MEA 2100-System, MCS) for both MH-MEA and 3D MC MEAs. The noise has been evaluated measuring the amplitude of the raw signals for each electrode of each MEA. Data were expressed as mean  $\pm$  standard deviation.

## 2.3. Human derived neurospheroids generation

Neurospheroids were generated by early-stage neurons and astrocytes. Specifically, early-stage neurons were obtained by the differentiation of h-iPSC into excitatory cortical layer 2/3 neurons by overexpressing the neuronal determinant neurogenin 2, upon doxycycline treatment as described previously [39]. Firstly, h-iPCs line (kindly provided by Frega *et al* [39]) were plated and maintained in culture on a six-well plate pre-coated with matrigel solution and cultured in essential eight flex (E8F) medium supplemented with essential eight flex supplement, 1% pen/strep, 50  $\mu\text{g ml}^{-1}$  G418 and 0.5  $\mu\text{g ml}^{-1}$  puromycin. The medium was refreshed every 2–3 d, and cells were passed twice weekly.

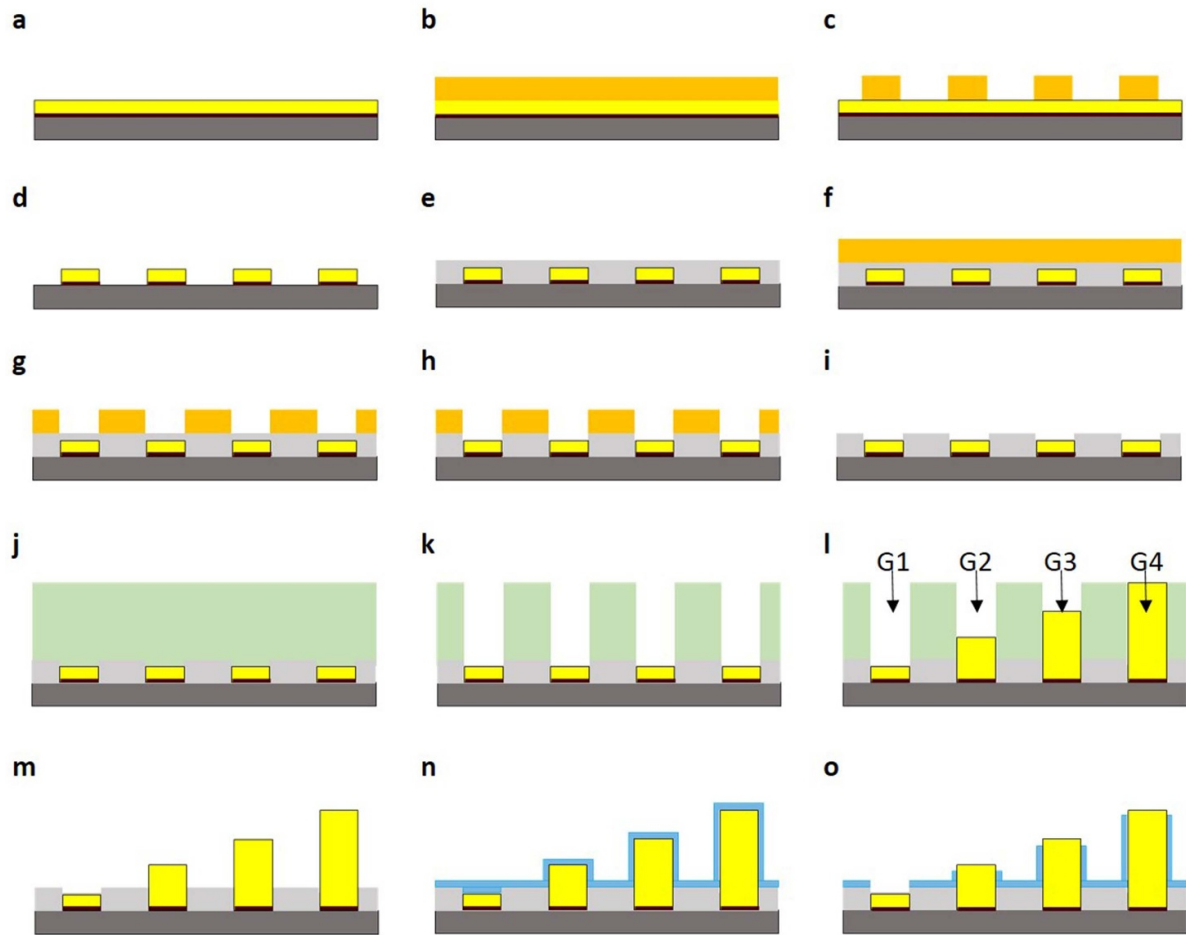


**Figure 2.** Fabrication process for multi-depth probing MEA. (a): Substrate i.e. glass wafer with 10 nm Cr and 200 nm Au layer. (b): Photoresist coated over the substrate. (c): Layout definition onto the photoresist. (d): Pattern transfer from photoresist to the metal layer on the substrate. (e): Deposition of passivation layer. (f): Photoresist coated over the passivation layer. (g): Pattern definition onto the photoresist. (h): Pattern transfer into the passivation layer. (i): Photoresist stripped to realize custom planar MEAs. (j): Photoresist (KMPR 1035) coated over the planar MEAs. (k): Definition of the photoresist mold. (l): Mold-assisted electrodeposition of gold micro-pillars. (m): Photoresist mold strip. (n): Deposition Parylene-C layer. (o): Removal of Parylene-C selectively from the top/head of the electrodes.

The neuronal differentiation was carried out as described in Shin *et al* [30]; briefly, h-iPSCs single-cell solution were plated *onto* matrigel pre-coated wells and cultured in *E8F + dox* medium ( $4 \mu\text{g m}^{-1}$  doxycycline (*Day 0*)). At *Day 1*, *E8F + dox* medium was completely replaced by DMEM/F12 supplemented with 1% MEM non-essential amino acid solution, 1% N2-supplement, 1% pens/strep,  $10 \text{ ng ml}^{-1}$  human-NT-3 and  $10 \text{ ng ml}^{-1}$  human-BDNF. On *Day 3*, cells (early-stage neurons) were collected and re-suspended in the medium, ready to be counted and used in co-culture for the neurospheroids generation. Astrocytes were obtained from primary cortical embryos (E18) as described in Aprile *et al* [40]. Neurospheroids were composed of  $8 \times 10^4$  early-stage neurons and astrocytes in a 1:1 ratio. Neurospheroids were generated by *hanging drop* method using a 5 cm petri dish as a ‘moisture chamber’. The petri dish was half-filled with Dulbecco’s phosphate-buffered saline (DPBS), and the inner part of the lid was used as sustain for the drops of the medium used as scaffold-free culture. Specifically, the lid has been inverted and  $15 \mu\text{l}$  drops of the neurobasal

medium were placed into the inner part of the lid; then,  $10 \mu\text{l}$  of the mixed-cells solution was added into each medium drop previously placed. Finally, the lid was gently placed back on the petri dish to avoid sliding of the drops and then stored it in the incubator at  $37^\circ\text{C}$  and  $5.5 \text{ CO}_2$ . This day was considered as the DIV 0 of the neurospheroids. At DIV 10, neurospheroids were moved into 24 well plates. Medium was supplemented with 2.5% of FBS and refreshed thrice weekly. At DIV 21, neurospheroids were moved onto the 3D MEAs.

#### 2.4. Preparation of MEAs

3D MC MEA (60-3DMEA250/12/100iR-Ti-gr) supplied by MCS was used as control. The 3D MC MEAs are glass devices with 60 titanium nitride electrodes embedded in the center of the culture well. They are arranged in an  $8 \times 8$  grid without electrodes at the corner, spaced  $250 \mu\text{m}$  among them, and are pyramidal with  $100 \mu\text{m}$  height and  $12 \mu\text{m}$  diameter tip. Before plating the neurospheroids, both 3D MEAs were cleaned and sterilized; 3D MC MEA were sterilized in an oven



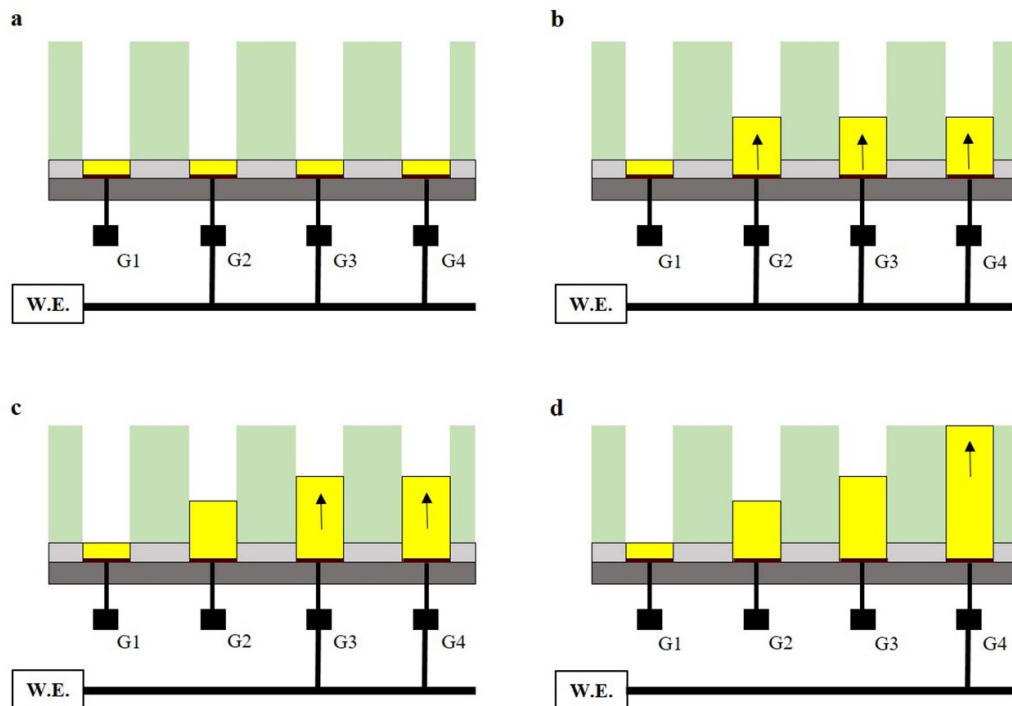


**Figure 3.** Mechanism for selective electrodeposition of gold micro-pillars. (a): Electrodes clubbed into different groups connected to the outer routing/working electrode (W.E.). (b): Stage-I electrodeposition, G2, G3, and G4 electrodes are electrodeposited simultaneously (indicated by upward arrows), and the process is terminated upon achieving desired height for G2 electrodes. (c): Stage-II electrodeposition for G3 and G4 electrodes. (d): Stage-III electrodeposition for G4 electrodes.

at 120 °C for two hours while MH-MEA was filled with 70% ethanol for 40 min. After that, the chambers were washed three times with  $\text{d}_2\text{H}_2\text{O}$ . Each chamber was filled with 2 ml DPBS, and the devices were stored in the incubator for two nights to improve the hydrophilicity of the substrate (conditioning phase). After this phase, all the devices were coated with a bi-layer composed of poly-L-ornithine (PLO, Sigma-Aldrich) and human-laminin (BioConnect). More specifically, 100  $\mu\text{l}$  of PLO solution (100  $\mu\text{g ml}^{-1}$ ) was placed on the active area of MEAs and then incubated at 4 °C overnight. The day after, the PLO solution was removed from the active area, washed twice with  $\text{d}_2\text{H}_2\text{O}$ , and then replaced with 80  $\mu\text{l}$  of laminin solution (20  $\mu\text{g ml}^{-1}$ ). Devices were then left overnight at 4 °C. The laminin solution was removed before plating the neurospheroids.

### 2.5. Electrophysiological recordings

The spontaneous electrophysiological activity (15 min) was recorded at DIV 29 using the ME2100-System (MEA 2100-System, MCS). Data were sampled at 10 kHz. Incubator-like conditions were maintained during recording by keeping the culture at 37 °C and 5.5%  $\text{CO}_2$  in sterile conditions.

### 2.6. Data analysis

Data analysis was performed by using a custom software package named SPYCODE, developed in MATLAB (The Mathworks, Natick, MA, USA) [22, 41–44]. Spike detection was performed using the precise timing spike detection

algorithm [42]. The algorithm requires three parameters: a different threshold set to eight times the standard deviation of the baseline noise, a peak lifetime period (set at 2 ms), and a refractory period (set at 1 ms). Raster plots showed an overview of the global activity recorded from each electrode of the MEA. The main parameters were extracted to characterize the electrophysiological activity: the mean firing rate (MFR), i.e. the number of spikes per second of each channel, and the percentage of random spikes, i.e. the fraction of spikes outside bursts. Moreover, burst detection was performed according to the method described in [43]. A burst is a sequence of spikes having an ISI (inter-spike interval, i.e. time intervals between consecutive spikes) smaller than a reference value (set at 100 ms in our experiments) and containing at least a minimum number of consecutive spikes (set at 5 spikes). The parameters extracted from this analysis were the mean bursting rate (MBR) and the mean burst duration (MBD), which are the frequency and duration of the bursts at the single channel level, respectively.

### 2.7. Morphological characterization

After the electrophysiological recordings, neurospheroids were fixed directly on the MEA at DIV 30 for immunofluorescence characterization. Samples were fixed using 4% paraformaldehyde solution for 20 min at room temperature and then washed three times in phosphate-buffered saline (PBS) solution. Samples were permeabilized with 0.2% triton X-100 for 15 min and then exposed to blocking buffer solution (0.5%

fetal bovine serum, 0.3% bovine serum albumin in PBS) for 45 min at room temperature, in order to block non-specific binding antibodies. GFAP (diluted 1:500) and MAP-2 (diluted 1:500) were used as primary antibodies to mark glial and neuronal cells, respectively, and Dapi (diluted 1:10 000) to label nuclei. Alexa Fluor 488 (diluted 1:700) and Alexa Fluor 546 (diluted 1:1000) Goat anti-mouse or Goat anti-rabbit were used as secondary antibodies.

### 2.8. Statistical analysis

We performed a non-parametrical Wilcoxon signed-rank test after evaluating the normality test carried out with GraphPad Prism. Differences were considered significant when  $p < 0.05$ .

## 3. Results

### 3.1. MH-MEA characteristics

To assess the technological platform we developed a MH-MEA containing 60 electrodes having a diameter of  $65 \mu\text{m}$  and a  $265 \mu\text{m}$  pitch, arranged in a hexagonal grid (figure 4(c)). The 60 electrodes in the array are categorized into four groups (G1, G2, G3, and G4) based on the electrode height relative to the substrate surface. The G1 electrodes have a planar topology, whereas G2, G3, and G4 electrodes consist of gold micro-pillars having heights of  $35 \pm 2 \mu\text{m}$ ,  $65 \pm 2 \mu\text{m}$ , and  $120 \pm 2 \mu\text{m}$  respectively (figure 4(b)), significantly taller than the previously reported 3D MEAs [28, 33, 36]. This unique distribution of electrode heights allowed the recording of electrophysiological activities from the surface to multiple depths within the neural culture (figure 4(i)).

Each electrode demonstrated capacitive behavior, with the impedance modulus decreasing linearly as a function of frequency on a log–log scale (figure 4(d), (top)). Meanwhile, the impedance phase maintained at around  $-80^\circ$  up to roughly 10 kHz, then decreased (figure 4(d), (bottom)). At 10 kHz, the planar electrodes (G1) had the highest impedance magnitude of  $17 \pm 1.64 \text{ k}\Omega$ , while the electrodeposited electrodes (G2, G3, and G4) had a much lower impedance magnitude ranging between 9.5–10.5 k $\Omega$  averaged over 10 number of electrodes from each group, comparable to state-of-the-art MEAs [25].

To assess electrode noise, the amplitude of the raw signals for each electrode was measured, and the average noise for each electrode group was calculated, as shown in figure 4(e). Furthermore, we contrasted the noise measured in two buffer solutions, PBS and medium culture (figure 4(f)). There were no statistical differences when comparing these two different conditions. The measurements performed with the 3D MC MEA provided similar results. Comparing the mean noise of all electrodes of MH-MEA and 3D MC MEA, with all 60 channels active, the mean noise values of the MH-MEA electrodes were higher compared to the 3D MC MEA. However, excluding the G1 electrodes of the MH-MEA resulted in a substantial overall reduction in noise, significantly lower than the 3D MC MEA (figure 4(g)).

### 3.2. Performance experimental evaluation in electrophysiological tests

The neurospheroids were plated on both types of 3D MEAs at 21 d *in-vitro* (DIV) after the complete formation of a 3D structure when neuronal and glial cells created a dense network with a spherical shape (figures 5(a) and (b)). Neurospheroids showed a mean diameter of around  $500 \mu\text{m}$ . The recording was performed one week after the plating to allow the full adhesion onto the 3D MEAs surface and ensure good interaction between cells and electrodes. Over time, neuronal processes enveloped the 3D electrodes while maintaining functional connections. The spontaneous activity (raw signal) of 1 s of a neurospheroid recorded from one micro-electrode of 3D MC and MH-MEA is shown in figures 5(c) and (d), respectively. A suitable resolution of the MH-MEA permits to clearly identify the onset of network events similar to what was observed with 3D MC MEA. The global electrophysiological behavior of a representative 3D network is shown in the raster plots of figure 5(e), where 15 min of spontaneous activities are displayed. In both MEA configurations (3D MC *on the top* and MH-MEA *on the bottom*), the activity recorded was related to a specific small group of electrodes ( $\sim 5$ – $8$ ). This was due to the dimension of the neurospheroid ( $500 \mu\text{m}$ ) that involved a low number of electrodes. Figures 5(f)–(i) show the parameters extracted from the analyzed spike data. Neurospheroids of 3D MC MEA presented values of MFR ( $0.80 \pm 0.06 \text{ spikes s}^{-1}$ ), different from the MH-MEA ( $0.47 \pm 0.04 \text{ spikes s}^{-1}$ ;  $p < 0.05$ ), figure 5(f). In both 3D MEA configurations, some electrodes were active even far away from the neurospheroids during the recording. For this reason, after the recordings, the 3D cultures were observed under the microscope, and we noticed that some cells moved out from the neurospheroids to other electrodes from which firing activity was detected. Both 3D experimental configurations detected high and comparable spiking activity values (figure 5(f)). Regarding the bursting behavior, the two MEA configurations shared similar values of MBR (figure 5(g)) and MBD (figure 5(h)); in particular, 3D MC MEA showed an MBR of  $2.4 \pm 0.57 \text{ (bursts min}^{-1}\text{)}$  and values of MBD round  $234.60 \pm 67.39 \text{ (ms)}$ ; while the values of MBR and MBD obtained by the MH-MEA recordings were around  $1.99 \pm 0.22 \text{ (bursts min}^{-1}\text{)}$  and  $214.83 \pm 13.19 \text{ (ms)}$  respectively.

This characterization indicated that MH-MEA could record spontaneous electrophysiological activity from mature human-derived neurospheroids, like the commercial 3D MC MEA. An indirect immunofluorescence technique was used to characterize neurospheroids onto the MH-MEA (figures 5(l) and (m)). To this purpose, the samples were prepared for indirect immunostaining at the end of the recording session. Morphological characterization confirmed and supported the results obtained by electrophysiological measures. In particular, 3D neurospheroids composed of human iPSC-derived cortical neurons and astrocytes have mostly retained their spherical shape, creating a packed network of neuronal and glial processes correctly plated onto the active area of

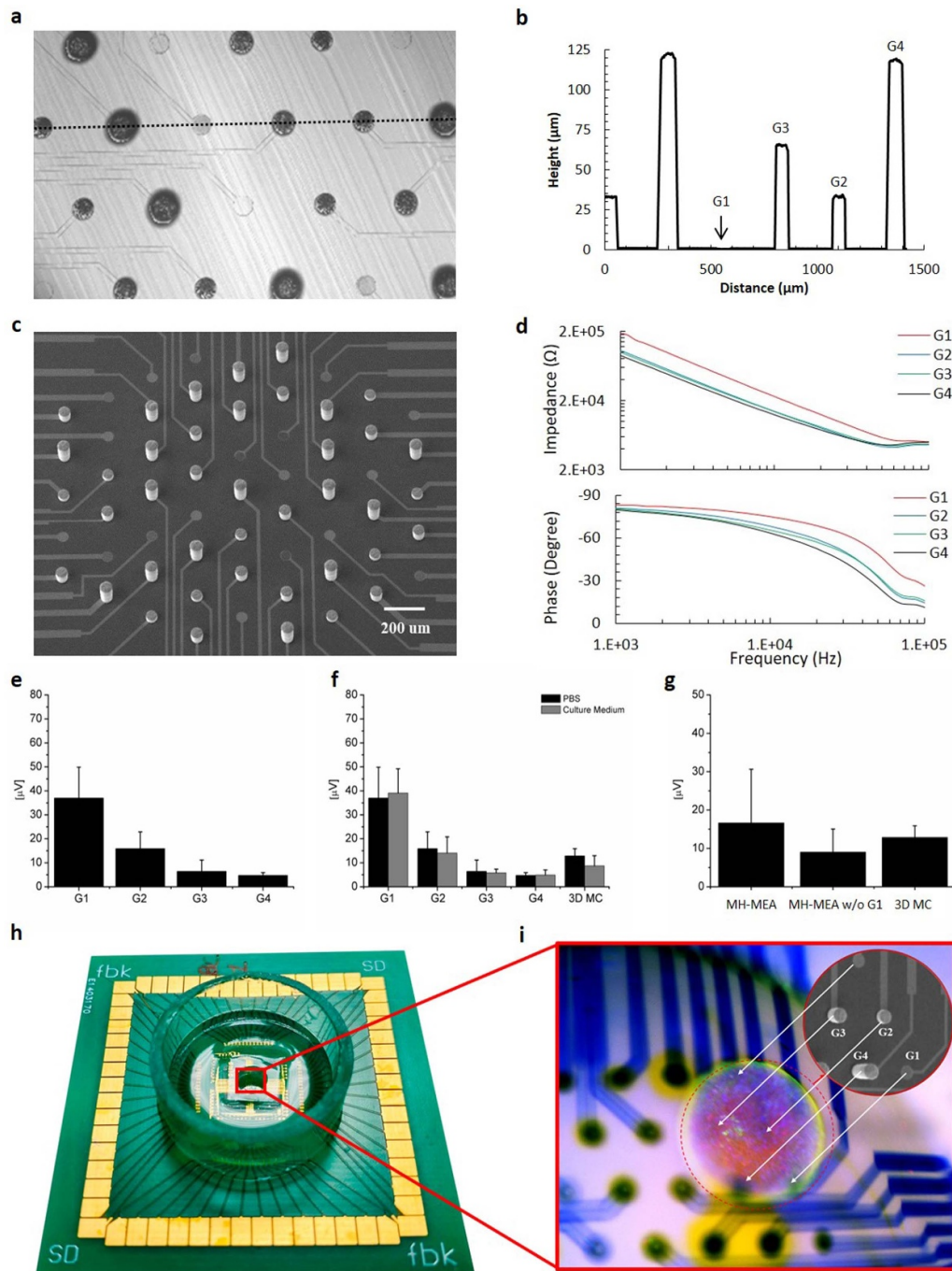


**Figure 4.** Device characteristics. (a): Optical scan image of the multi-depth probing electrode array obtained using optical profilometer. (b): Height profile of the electrodes extracted along the dashed line in figure 4(a). (c): SEM image of fabricated multi-depth probing MEA consisting of 60 electrodes ranging from planar to 120  $\mu\text{m}$  tall micro-pillars having a radius of 32.5  $\mu\text{m}$ . (d): Impedance spectra ranging between 1 kHz–100 kHz, magnitude of impedance (top) and phase (bottom) vs. the frequency range ( $n = 5$ , where  $n$  is the number of electrodes analyzed for each group). (e): Comparison of mean noise of different electrode groups simultaneously. (f): Comparison of mean noise of MH-MEA electrode groups ( $n = 60$ ) and 3D MC with all the active channels ( $n = 60$ ) in PBS and medium culture. (g): Comparison of mean noise of MH-MEA with and w/o G1 ( $n = 41$ ) electrodes and 3D MC. (h): Fully assembled MH-MEA. (i): enlarged image of the cell culture well, showing neurospheroid (encircled in red dashed line) plated over electrodes with different heights, image taken at DIV 29.

3D MEA. In fact, the position of the neurospheroids corresponded to the active electrodes from which the spontaneous activity was recorded, figure 5(l). The presence of neurons and astrocytes was confirmed by positive staining

with microtubule-associated protein 2 (MAP-2), a protein highly expressed in neurons, and glial fibrillary acidic protein (GFAP), a protein expressed by astrocytes. Confocal microscopy characterization allowed us to gain information



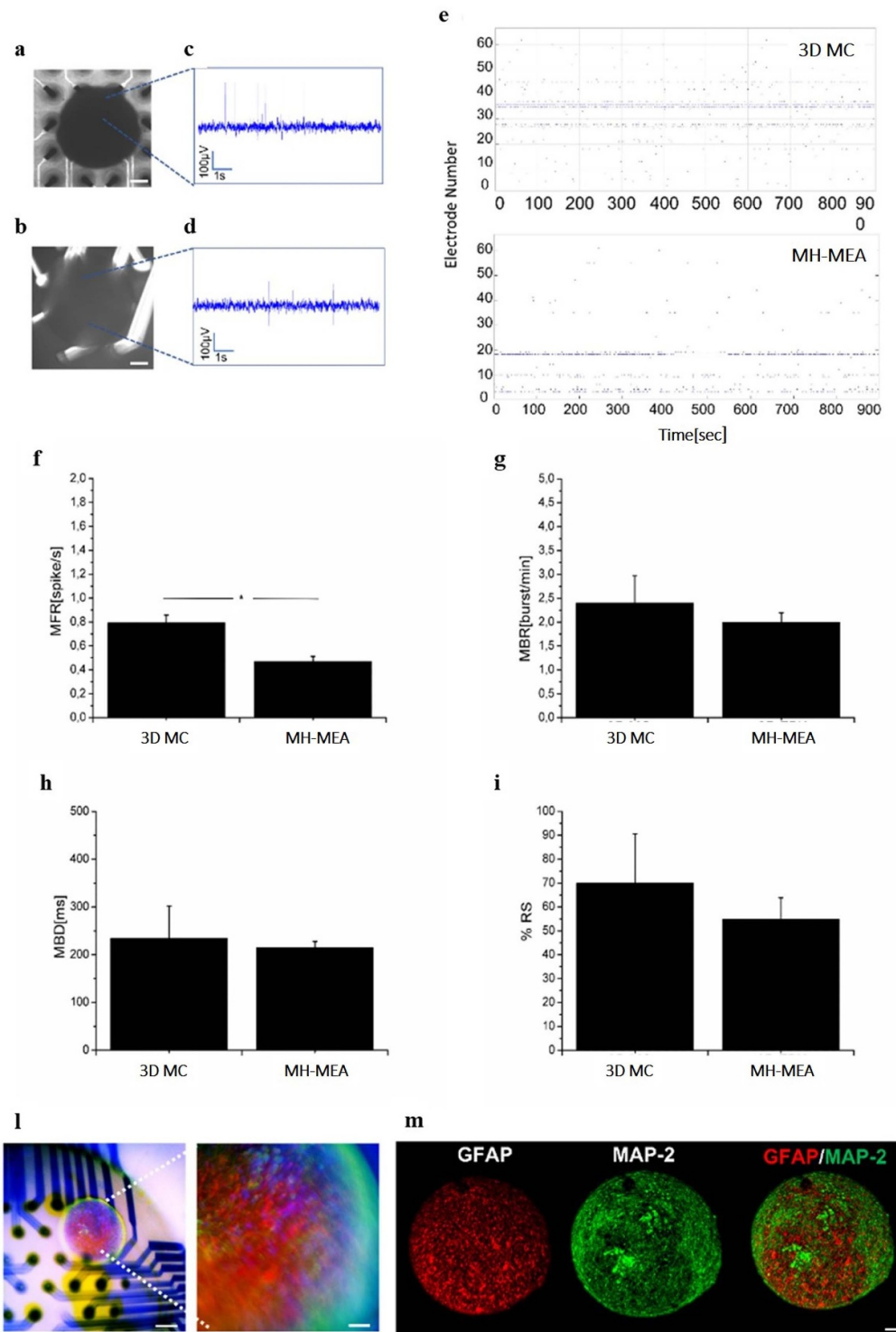


**Figure 5.** Optical images showing neurospheroid at DIV 25 on, (a): 3D MC MEA (scale: 100  $\mu\text{m}$ ) and (b): MH-MEA (scale: 100  $\mu\text{m}$ ). Raw data trace recorded by one electrode placed below the neurospheroid plated on (c): 3D MC MEA, (d): MH-MEA. Analysis of the spontaneous activity, (e): raster plots showing 15 min of activity recorded by 3D MC MEA and MH-MEA. Graphs showing, (f): mean firing rate, (g): mean bursting rate (MBR), (h): mean burst duration (MBD), (i): percentual random spikes (%RS) ( $n = 5$ , where  $n$  is number of electrodes actively recording the electrophysiological signals for each MEA). (l): Fluorescence images of neurospheroid on MH-MEA and zoom of the same neurospheroid at DIV 30 marked for MAP-2 (green), GFAP (red), and DAPI (blue). Scale bar: 250  $\mu\text{m}$ , 100  $\mu\text{m}$ . (m): Confocal images; max projection of neurospheroid at DIV 30 labeled for GFAP (red), MAP-2 (green), and merge—scale bar: 50  $\mu\text{m}$ .

on the morphology of the 3D structure of mature neuronal distribution of neural cells on the surface and interior of the neurospheroids, figure 5(m). Specifically, the max projection obtained by a 3D reconstruction of 240  $\mu\text{m}$  z-stack of the human neurospheroids immunolabeled for the dendritic marker MAP-2 and GFAP gave us a comprehensive view of the 3D neural structure (video 1), indicating that the MH-MEA supported healthy neurospheroids cultures that were not affected by any materials present in the 3D MEA arrays.

#### 4. Conclusion and future directions

We presented the successful development and application of an innovative technological platform for the production of multi-depth probing 3D MEAs. The fabrication process consistently created 60-channel MH-MEA devices, each with electrodes organized into four groups based on electrode heights. The results demonstrated the electrodes' low electrochemical impedance and noise measurement properties in all four groups. The measurements provided valuable insights into the behavior of the electrodes across a range of frequencies. They further highlighted the potential of the fabricated MH-MEAs for advanced electrophysiological studies. In electrophysiological activity recordings, the multi-depth probing MH-MEA showed efficacy in monitoring the electrophysiological activity of a 3D neuronal culture. The ability to record spontaneous electrophysiological activity from mature human-derived neurospheroids comparable to a commercial 3D MC MEA was an encouraging outcome. This opens up new possibilities in neuroscience, particularly in studying complex neuronal activities in a 3D setup.

#### Data availability statement

All data that support the findings of this study are included within the article (and any supplementary files).

#### Acknowledgments

This work was partially funded by European Union (NextGeneration EU) through the MUR-PNRR project SAMOTHRACE (ECS00000022). We want to thank Dr Andrea Spanu of Advanced Electronic Devices LABORatory (DEALAB), University of Cagliari, for the deposition of Parylene-C. We would like to acknowledge the PhD Thesis of Lorenzo Muzzi entitled 'Development of engineered human-derived brain-on-a-chip models for electrophysiological recording' for the protocol to generate and electrophysiological characterization of Neurospheroids.

#### Ethical statement

The experimental protocol was approved by the European Animal Care Legislation (2010/63/EU), by the Italian Ministry of Health in accordance with the D.L. 116/1992 and by the guidelines of the University of Genova.

#### Conflict of interest

The authors declare no competing interests.

#### ORCID iDs

Neeraj Yadav  <https://orcid.org/0000-0002-2159-7016>  
Flavio Giacomozzi  <https://orcid.org/0000-0002-6009-0103>

#### References

- [1] Pine J 2006 A history of MEA development *BT Advances in Network Electrophysiology: Using Multi-Electrode Arrays* ed M Taketani and M Baudry (Springer) pp 3–23
- [2] McCreedy F P, Gordillo-Sampedro S, Pradeepan K, Martinez-Trujillo J and Ellis J 2022 Multielectrode arrays for functional phenotyping of neurons from induced pluripotent stem cell models of neurodevelopmental disorders *Biology* **11** 316
- [3] Morris-Rosendahl D J and Crocq M-A 2019 Dialogues in clinical neuroscience neurodevelopmental disorders—the history and future of a diagnostic concept *Clin. Neurosci.* **22** 65–72
- [4] Ogawa S, Lee T M, Kay A R and Tank D W 1990 Brain magnetic resonance imaging with contrast dependent on blood oxygenation *Proc. Natl Acad. Sci. USA* **87** 9868
- [5] Logothetis N K, Pauls J, Augath M, Trinath T and Oeltermann A 2001 Neurophysiological investigation of the basis of the fMRI signal *Nature* **412** 150–7
- [6] Schomer D L and da Silva F H L 2005 *Niedermeyer's Electroencephalography: Basic Principles, Clinical Applications, and Related Fields* vol 1 (Lippincott and Wilkins)
- [7] Buzsáki G, Anastassiou C A and Koch C 2012 The origin of extracellular fields and currents—EEG, ECoG, LFP and spikes *Nat. Rev. Neurosci.* **13** 407–20
- [8] Buzsáki G, Logothetis N and Singer W 2013 Scaling brain size, keeping timing: evolutionary preservation of brain rhythms *Neuron* **80** 751–64
- [9] Lancaster M A, Renner M, Martin C-A, Wenzel D, Bicknell L S, Hurler M E, Homfray T, Penninger J M, Jackson A P and Knoblich J A 2013 Cerebral organoids model human brain development and microcephaly *Nature* **501** 373–9
- [10] Wang Y et al 2023 Emerging trends in organ-on-a-chip systems for drug screening *Acta Pharm. Sin. B* **13** 2483–09
- [11] Trujillo C A and Muotri A R 2018 Brain organoids and the study of neurodevelopment *Trends Mol. Med.* **24** 982–90
- [12] Ravi M, Paramesh V, Kaviya S R, Anuradha E and Paul Solomon F D 2015 3D cell culture systems: advantages and applications *J. Cell. Physiol.* **230** 16–26

- [13] Breslin S and O'Driscoll L 2013 Three-dimensional cell culture: the missing link in drug discovery *Drug Discov. Today* **18** 240–9
- [14] Yang X, Zhou T, Zwang T J, Hong G, Zhao Y, Viveros R D, Fu T-M, Gao T and Lieber C M 2019 Bioinspired neuron-like electronics *Nat. Mater.* **18** 510–7
- [15] Pas S P 2018 The rise of three-dimensional human brain cultures *Nature* **553** 437–45
- [16] Hopkins A M, DeSimone E, Chwalek K and Kaplan D L 2015 3D *in vitro* modeling of the central nervous system *Prog. Neurobiol.* **125** 1–25
- [17] Engelen M, Obien M E J, Deligkaris K, Bullmann T, Bakkum D J and Frey U 2015 Revealing neuronal function through microelectrode array recordings *Front. Neurosci.* **8** 423
- [18] Ylä-Outinen L et al 2010 Human cell-based micro electrode array platform for studying neurotoxicity *Front. Neuroeng.* **3** 6927
- [19] Dauth S, Maoz B M, Sheehy S P, Hemphill M A, Murty T, Macedonia M K, Greer A M, Budnik B and Parker K K 2017 Neural circuits: neurons derived from different brain regions are inherently different *in vitro*: a novel multiregional brain-on-a-chip *J. Neurophysiol.* **117** 1320
- [20] Fendyur A and Spira M E 2012 Toward on-chip, in-cell recordings from cultured cardiomyocytes by arrays of gold mushroom-shaped microelectrodes *Front. Neuroeng.* **5** 1–10
- [21] Berdondini L, Imfeld K, Maccione A, Tedesco M, Neukom S, Koudelka-Hep M and Martinoia S 2009 Active pixel sensor array for high spatio-temporal resolution electrophysiological recordings from single cell to large scale neuronal networks *Lab Chip* **9** 2644
- [22] Muzzi L, Di Lisa D, Arnaldi P, Aprile D, Pastorino L, Martinoia S and Frega M 2021 Rapid generation of functional engineered 3D human neuronal assemblies: network dynamics evaluated by micro-electrodes arrays *J. Neural Eng.* **18** 066030
- [23] Choi J S, Lee H J, Rajaraman S and Kim D-H 2021 Recent advances in three-dimensional microelectrode array technologies for *in vitro* and *in vivo* cardiac and neuronal interfaces *Biosens. Bioelectron.* **171** 112687
- [24] Decker D, Hempelmann R, Natter H, Pirrung M, Rabe H, Schäfer K H and Saumer M 2019 3D nanostructured multielectrode arrays: fabrication, electrochemical characterization, and evaluation of cell–electrode adhesion *Adv. Mater. Technol.* **4** 1800436
- [25] Weidlich S, Krause K J, Schnitker J, Wolfrum B and Offenhäuser A 2017 MEAs and 3D nanoelectrodes: electrodeposition as tool for a precisely controlled nanofabrication *Nanotechnology* **28** 095302
- [26] Bertotti G, Jetter F, Keil S, Dodel N, Schreiter M, Wolansky D, Boucsein C, Boven K-H, Zeck G and Thewes R 2017 Optical stimulation effects on TiO<sub>2</sub> sensor dielectric used in capacitively-coupled high-density CMOS microelectrode array *IEEE Electron Device Lett.* **38** 967–70
- [27] Saleh M S et al 2022 CMU array: a 3D nanoprinted, fully customizable high-density microelectrode array platform *Sci. Adv.* **8** eabj4853
- [28] Spanu A, Colistra N, Farisello P, Friz A, Arellano N, Rettner C T, Bonfiglio A, Bozano L and Martinoia S 2020 A three-dimensional micro-electrode array for *in-vitro* neuronal interfacing *J. Neural Eng.* **17** 036033
- [29] Goncalves S B, Peixoto A C, Silva A F and Correia J H 2015 Fabrication and mechanical characterization of long and different penetrating length neural microelectrode arrays *J. Micromech. Microeng.* **25** 055014
- [30] Shin H, Jeong S, Lee J-H, Sun W, Choi N and Cho I-J 2021 3D high-density microelectrode array with optical stimulation and drug delivery for investigating neural circuit dynamics *Nat. Commun.* **12** 492
- [31] Didier C M, Kundu A, Deroo D and Rajaraman S 2020 Development of *in vitro* 2D and 3D microelectrode arrays and their role in advancing biomedical research *J. Micromech. Microeng.* **30** 103001
- [32] Teixeira H, Dias C, Aguiar P and Ventura J 2021 Gold-mushroom microelectrode arrays and the quest for intracellular-like recordings: perspectives and outlooks *Adv. Mater. Technol.* **6** 2000770
- [33] Steins H et al 2022 A flexible protruding microelectrode array for neural interfacing in bioelectronic medicine *Microsyst. Nanoeng.* **8** 131
- [34] Soscia D A, Lam D, Tooker A C, Enright H A, Triplett M, Karande P, Peters S K G, Sales A P, Wheeler E K and Fischer N O 2020 A flexible 3-dimensional microelectrode array for: *in vitro* brain models *Lab Chip* **20** 901–11
- [35] Spira M E and Hai A 2013 Multi-electrode array technologies for neuroscience and cardiology *Nat. Nanotechnol.* **8** 83–94
- [36] Yadav N, Lorenzelli L and Giacomozzi F 2021 A novel additive manufacturing approach towards fabrication of multi-level three-dimensional microelectrode array for electrophysiological investigations 2021 23rd European Microelectronics and Packaging Conf. & Exhibition (EMPC) (IEEE) pp 1–5
- [37] Shin S-B et al 2023 Fabrication of a transparent array of penetrating 3D microelectrodes with two different heights for both neural stimulation and recording *Sens. Actuators B* **393** 134184
- [38] Roh H, Yoon Y J, Park J S, Kang D-H, Kwak S M, Lee B C and Im M 2022 Fabrication of high-density out-of-plane microneedle arrays with various heights and diverse cross-sectional shapes *Nano-Micro Lett.* **14** 1–19
- [39] Frega M, Jokivarsi K T, Knight M J, Grohn O H J and Kauppinen R A 2017 Rapid neuronal differentiation of induced pluripotent stem cells for measuring network activity on micro-electrode arrays *J. Vis. Exp.* **2017** e54900
- [40] Aprile D et al 2019 TBC1D24 regulates axonal outgrowth and membrane trafficking at the growth cone in rodent and human neurons *Cell Death Differ.* **26** 2464–78
- [41] Bologna L L, Pasquale V, Garofalo M, Gandolfo M, Baljon P L, Maccione A, Martinoia S and Chiappalone M 2010 Investigating neuronal activity by SPYCODE multi-channel data analyzer *Neural Netw.* **23** 685–97
- [42] Maccione A, Gandolfo M, Massobrio P, Novellino A, Martinoia S and Chiappalone M 2009 A novel algorithm for precise identification of spikes in extracellularly recorded neuronal signals *J. Neurosci. Methods* **177** 241–9
- [43] Pasquale V, Martinoia S and Chiappalone M 2010 A self-adapting approach for the detection of bursts and network bursts in neuronal cultures *J. Comput. Neurosci.* **29** 213–29
- [44] Tedesco M T, Di Lisa D, Massobrio P, Colistra N, Pesce M, Catelani T, Dellacasa E, Raiteri R, Martinoia S and Pastorino L 2018 Soft chitosan microbeads scaffold for 3D functional neuronal networks *Biomaterials* **156** 159–71